Heliyon 9 (2023) e23004

Contents lists available at ScienceDirect

Heliyon

journal homepage: www.cell.com/heliyon

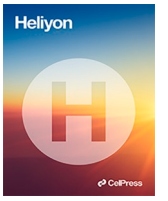

Pyroptosis-related gene signature: A predictor for overall survival, immunotherapy response, and chemosensitivity in patients with pancreatic adenocarcinoma

Jieting Zhou, Jian Fan *, Binxiao Li, Jiayu Sun, Jingchao Wang

Department of Laboratory Medicine, The First Affiliated Hospital, Zhejiang University School of Medicine, Hangzhou, China

ARTICLE INFO

Keywords:
Pancreatic adenocarcinoma
Pyroptosis
Immunotherapy

ABSTRACT

Background: Pancreatic adenocarcinoma (PAAD) is a lethal malignancy with high levels of heterogeneity. Pyroptosis is thought to influence the development of various tumors. Nevertheless, the role of pyroptosis-related genes (PRGs) in prognostic risk stratification and therapeutic guidance for PAAD remains ambiguously.

Methods: Transcriptome profile and clinical information of PAAD patients were retrieved from The Cancer Genome Atlas (TCGA) as well as Gene Expression Omnibus (GEO) databases, followed by differential analysis. Patients were divided into distinct pyroptosis phenotype subtypes based on the characteristic of differently expressed PRGs (DEPRGs). Then a PRG signature was established through univariate analysis and LASSO algorithm in the training set to assess the prognostic risk, and its reliability was verified in the validation set using receiver operating characteristic(ROC) curve. The correlation of risk score with tumor microenvironment(TME), TMB and chemotherapeutic drug sensitivity were also analyzed. In addition, a nomogram was constructed to promote better clinical application.

Results: A total of 28 DEPRGs were determined in the integrated TCGA-GEO datasets. Patients were divided into three pyroptosis phenotype subtypes, Kaplan-Meier curve suggested patients in cluster B had a worse prognosis than those in cluster A and C. Then a price signature comprised of 8 PRGs was generated. TME analysis suggested that the low-risk subgroup displayed potential stronger antitumor immune effect and might respond better to immune checkpoint inhibitors (ICIs) therapy. Furthermore, PRG signature exhibited favorable discriminatory ability for TMB status and the sensitivity of multiple conventional chemotherapeutic agents including paclitaxel. Ultimately, we constructed a promising nomogram according to the risk score and N stage with good predictive accuracy compared with the actual overall survival (OS) probabilities.

Conclusion: We established an 8-gene signature that could be regarded as an independent prognostic risk factor for PAAD patients. The 8-gene signature could provide rationale for immunotherapy and chemotherapy, which might help clinicians make precise individualized treatment regimens.

* Corresponding author.
E-mail address: 3319fanjian@163.com (J. Fan).

https://doi.org/10.1016/j.heliyon.2023.e23004
Received 10 April 2023; Received in revised form 13 November 2023; Accepted 23 November 2023
Available online 28 November 2023

1. Introduction

Pancreatic adenocarcinoma is one of the most fatal malignancies with approximately 9 % 5-year overall survival rate and 6–8 months median survival time after diagnosis [1]. It currently ranks seventh among the causes of cancer mortality worldwide and is estimated to raise to the second by 2030 [2,3]. Generally, surgical resection is considered the most effective potential curative treatment, which significantly elevates the 5-years survival rate of early stage patients to 24.6 % [4].However, majority of PAAD patients miss the chance for operation at first diagnosis owing to absence of early detection methods and recognizable symptoms [5]. For these patients with unresectable or postoperative status, conventional chemotherapies such as FOLFIRINOX and Nab-Gem are the main therapeutic options, but the effectiveness is unsatisfactory [6]. In the past decades, despite advances in several treatment strategies including adjuvant chemotherapies, targeted therapies and immunotherapies have been developed, the PAAD is still characterized by poor prognosis and presents a disparity in the resistance to multiple therapeutic methods [7]. The vital cause of disparities in clinical outcome and response to treatments between PAAD patients is significantly associated with molecular complexity and heterogeneity between their tumors. However, survival prediction and selection of systemic therapies were largely depending on the American Joint Committee on Cancer (AJCC) classification system and histopathology type, which could not meet the needs of clinicians to initiate personalized treatment protocol [8]. Thus, it is a critical thing to develop a novel prognostic model to help clinicians accurately evaluate the survival outcome of PAAD patients and optimize medical regimen.

Pyroptosis is a pro-inflammatory mode of programmed cell death induced by microbial invasion, malignant neoplasms and other pathophysiological stimuli [9]. The specific characteristics of pyroptosis distinguished from apoptosis is chromatin laddering, plasma membrane perforation, cytoplasmic swelling with bubble-like protrusions and subsequent cellular lysis combined with release of intracellular cytokines [10,11]. Caspases family proteins and gasdermin family proteins are essential “executioners” during pyroptosis process [12]. In the canonical pyroptosis pathways, stimulated by pathogen-associated molecular patterns (PAMPs) or damage-associated molecular patterns(DAMPs), inflammasomes defined as cytoplasmic multi-protein platform containing the pattern-recognition receptors (PRRs) is assembled, which activated the pro-caspase-1 [13]. In the noncanonical pyroptosis process, caspase-4/5 could be activated via N-terminal recruitment domain directly binding to the intracytoplasmic lipopolysaccharide (LPS) generated by invading gram-negative bacteria [14]. Subsequently, the activated caspase-1/4/5 could cut GSDMD into the N-terminal and C-terminal fragment and promoted release of mature IL-1β and IL-18, while the GSDMD N-terminal will oligomerize and structure 10–20 nm pores in cell layer [15,16]. Besides, other vicarious pathways that depends on caspase-3/GSDME or granzyme-A/GSDMB have been also identified to induce pyroptosis [17,18].

Recently, a rising number of studies have illustrated the role and mechanism of pyroptosis malignant tumor, although the connection between pyroptosis and tumor prognosis is still debatable, this is due to the possibility that pyroptosis might have a dual role in the development of carcinoma. The pyroptosis of cancer cells could efficiently supress the proliferation and metastasis of malignant tumors, and the immune system could be stimulated to work better against tumors [19]. On the contrary, the proinflammatory cell death induced by pyroptosis could accelerate immune evasion and facilitate a suitable tumor microenvironment for tumor growth [20]. To date, the survival predicting ability of pyroptosis-related signature has been extensively studied in multiple tumor types including lung adenocarcinoma(LUAD) [21], hepatocellular cancer [22] and gliomas [23].Unfortunately, the clinical prognostic significance of pyroptosis in PAAD is still unclarified.

In our research, combined with machine learning algorithm, we verified the differences in prognosis between distinct pyroptosis phenotype subtypes and established a PRG signature. We also evaluated the OS rate between patients with high- and low-risk and explored the possible biological mechanism. In addition, we analyzed the connection between PRG signature, TME, mutation landscape and IC50 of chemotherapeutic drug. Our study is intended to investigate the role of PRGs in prognostic risk stratification and evaluate the predictive power of this risk stratification signature in relation to the chemotherapeutic agent sensitivity and immunotherapy efficacy for PAAD patients with different risk groups. We hope our study offer reference advice for the precise prognostic management of PAAD patients.

2. Materials and methods

2.1. Data acquirement and preparation

Transcriptome data and relevant clinical features of 182 PAAD patient samples were retrieved from TCGA data portal through UCSC Xena platform (http://xena.ucsc.edu/; version 2018-07-22). Two samples with incomplete survival data or TNM stage information were excluded. Thus, 176 PAAD samples and 4 normal adjacent samples were enrolled.

Besides, another 220 PAAD patient samples from two datasets were auquired from the GEO data portal (https://www.ncbi.nlm.nih.gov/geo/). The microarray data of GSE28735 and GSE62452 were based on GPL6244 Platform, including 45 tumor tissue samples,45 normal adjacent tissue samples and 69 tumor tissue samples,61 adjacent normal tissue samples respectively.

The three datasets were merged by removing the batch effect using “sva” package [24] and generated a larger combined cohort for follow-up bioinformatics analysis.

Transcriptome data and clinical information of advanced urothelial carcinoma patients who underwent anti-PD-L1 therapy from IMvigor210 cohort was retrieved from http://research-pub.gene.com/.

2.2. Identification of DEPRGs

The differentially expressed genes (DEGs) between primary tumor and normal adjacent samples was assessed throug the "limma" R package, selecting by the threshold of p value < 0.05 [25]. 47 PRGs were extracted from the MsigDB (http://www.broadinstitute.org/msigdb) and earlier reviews. The intersection between DEGs and PRGs were regarded as DEPRGs and then visualized via "pheatmap" R package.

2.3. DEPRGs consensus clustering

An unsupervised Consensus clustering analysis was carried out utilizing ConsensusClusterPlus package [26] to divide PAAD tumor samples into distinct pyroptosis phenotype subtypes according to the expression matrix of the DEPRGs. The appropriate number of PAAD subtype with stable sample distribution was identified by the cumulative distribution function (CDF) curve and optimal k means [27]. To compare survival time between pyroptosis phenotype subtypes, Kaplan-Meier curve was conducted using "survival" as well as "survminer" R packages [28].

2.4. Establishment and assessment of prognostic risk signature

TCGA-PAAD ($n = 176$) was utilized as a training set, and the combined TCGA-GEO cohort ($n = 220$) was taken as a validation set. To begin with, univariate Cox regression analysis was performed to screen out DEPRGs linked to OS in training set, and only DEPRGs with a p value < 0.05 were considered as candidates for the creation of prognostic risk signature [29]. Further, these pre-selected genes were subjected to LASSO regression algorithm with application of "glmnet" R package, followed by the determination of optimum penalty parameter lamba (λ) through tenfold cross-validation. Ultimately, core prognostic genes included in the signature and corresponding coefficient was obtained from multivariate COX regression analysis. The risk score was calculated as following formula: $\sum_{k=0}^{n} Coef_k \; Exp_k$.

$Coef_k$ suggests regression coefficient, while Exp_k is the expression quantity of each signature gene. According to whether risk score was above or below the median, patients were distributed to two subgroups. Kaplan–Meier curve was drawn to assess the OS between two risk subgroups, showing the efficiency of core prognostic genes. Meanwhile, ROC curve was plotted to appraise prognostic prediction performance of our PRG signature using "timeROC" R package. The above formula and same evaluation method was also applied in the validation set.

2.5. Functional annotation analysis of DEGs between subgroups at high- and low-risk

By using "Deseq2" R package, DEGs comparing around risk subgroups (high-versus low-risk group) were discovered, p-value<0.05 together with $|\log FC|>1$ was chosen as the criteria. Expression features of DEGs with statistical significance were displayed via heatmap and volcano plot using "pheatmap" and "ggplot2" R package.

To demonstrate the functional annotations of risk score related DEGs, "clusterProfiler" R package was applied to conduct Gene ontology (GO) and Kyoto Encyclopedia of Genes and Genomes (KEGG) analysis [30], the results with p-value <0.05 in conjunction with q-value <0.05 was defined as significant enrichment. In addition, the functional vlaue of DEGs in the most significant pathway was rated by semantic similarity algorithms using "GoSemSim" R package [31].

2.6. Gene set enrichment analysis (GSEA)

To investigate the underlying molecular pathway cause that responsible for the disparity in survival outcome between risk subgroups, GSEA was applied for analysis of the significantly enriched pathways using "clusterProfiler" R package. The pre-defined gene set "H.all.v7.4. entrez" was obtained from MSigDB database, and only pathways with p-value <0.05 were marked as statistical significantly.

2.7. PPI network construction

DEGs between risk subgroups were uploaded onto the Search Tool for the Retrieval of Interacting Genes (STRING) online database (https://cn.string-db.org/) to assess protein–protein interactions (PPIs) information. Confidence score ≥ 0.700 was set as a threshold. Cytoscape software (v3.8.0) was applied to show PPI network based on STRING results. CytoHubba plug-in was utilized to identify significant protein nodes and submodules of PPI network. The top 20 hub genes were chosen through edge percolated component (EPC) algorithm, and the interaction relationship of them was displayed.

2.8. Construction of miRNA-DEGs regulatory network

The regulatory factor miRNAs of DEGs differ across risk subgroups were predicted using "multiMIR" R package [32], which contained miRNA-mRNA target interaction information from 14 databases including 3 verified databases, 8 predicted databases and 3 miRNA-disease/drug association databases. The obtained miRNA-DEGs pairs that validated by luciferase reporter assays in

miRTarBase database were selected to establish the miRNA-DEGs regulatory network, followed by visualization using Cytoscape software. Furthermore, miRNA-DEGs interaction that contained the top 20 hub genes was extracted to visualize through "ggalluvial" R package.

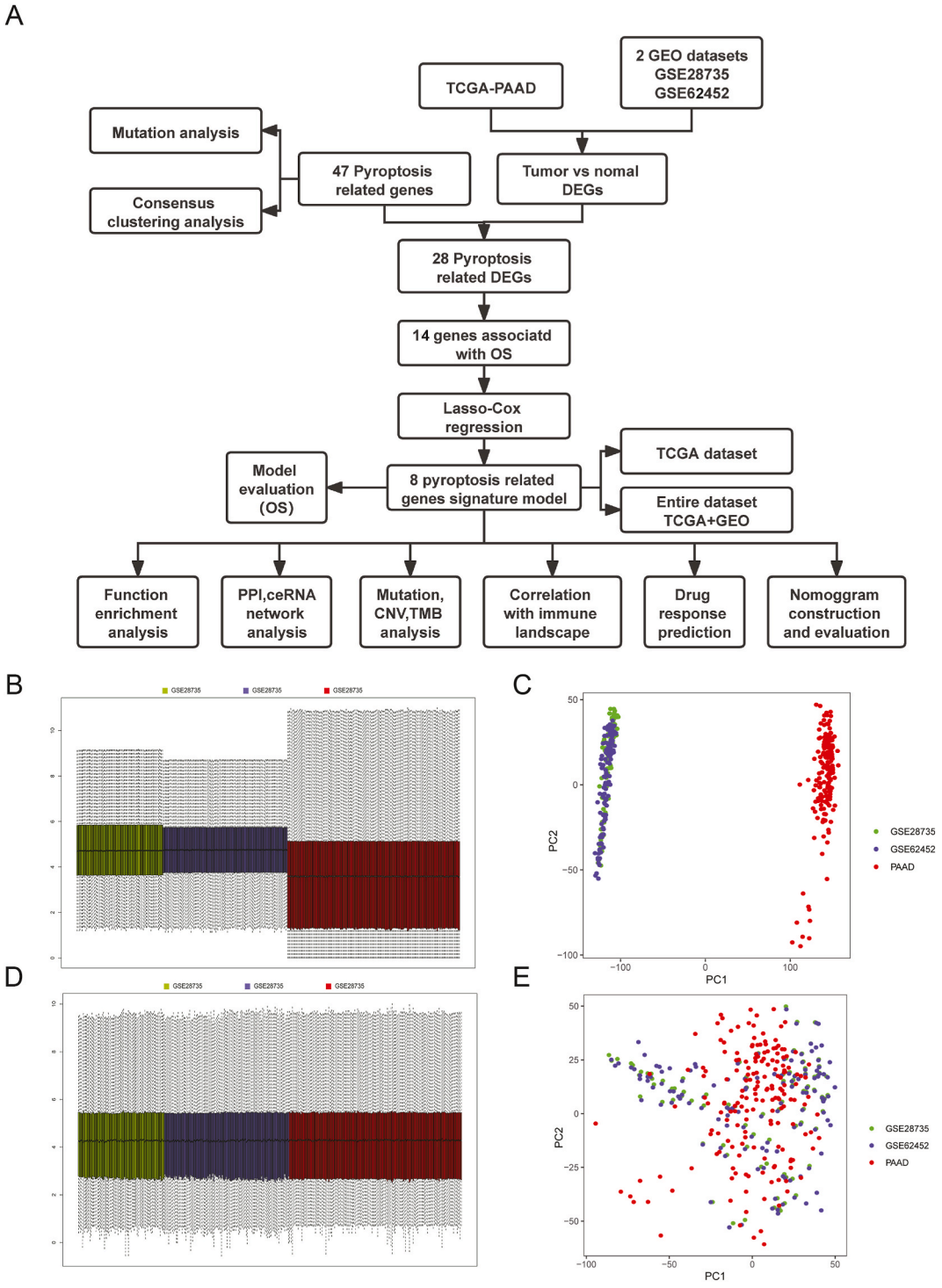

Fig. 1. Whole process of our research and elimination of batch effect between datasets (A) Flow diagram describing data collection and processing (B,C) The box and PCA plot of three datasets without batch effect elimination (D,E) The box and PCA plot of three datasets with removal of batch effect.

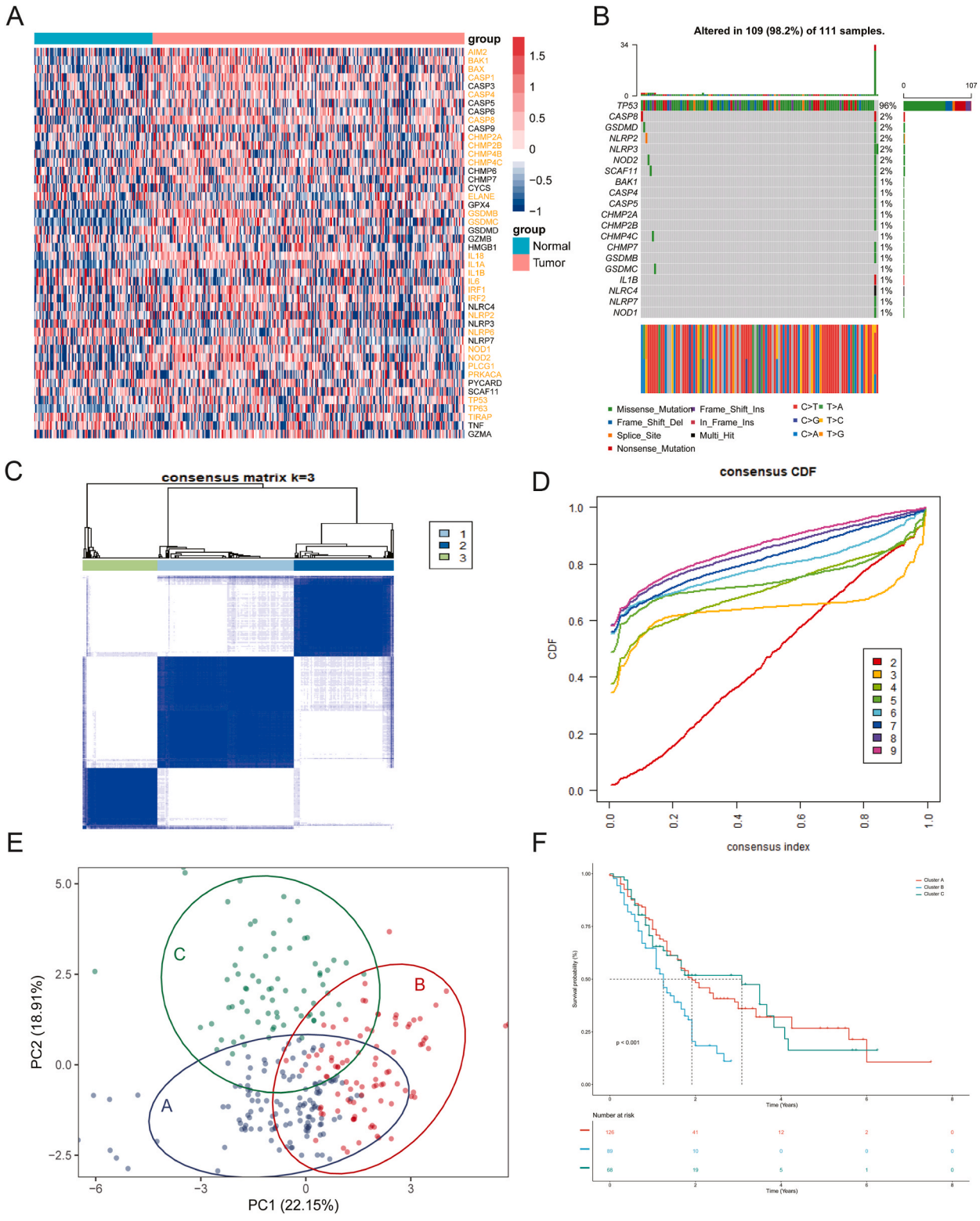

Fig. 2. | Determination of DEPRGs and pyroptosis phenotype subtypes using unsupervised clustering analysis (A) Heatmap of 46 PRGs expression in tumor and normal adjacent tissues, genes with yellow font represents the DEPRGs (B) The mutation characteristics of PRGs in TCGA-PAAD cohort (C) Consensus matrix heatmap for k = 3 in PAAD (D) CDF curve when k changing from 2 to 9 (E) PCA plot of three pyroptosis phenotype clusters (F) Kaplan-Meier curve for OS between three pyroptosis phenotype clusters

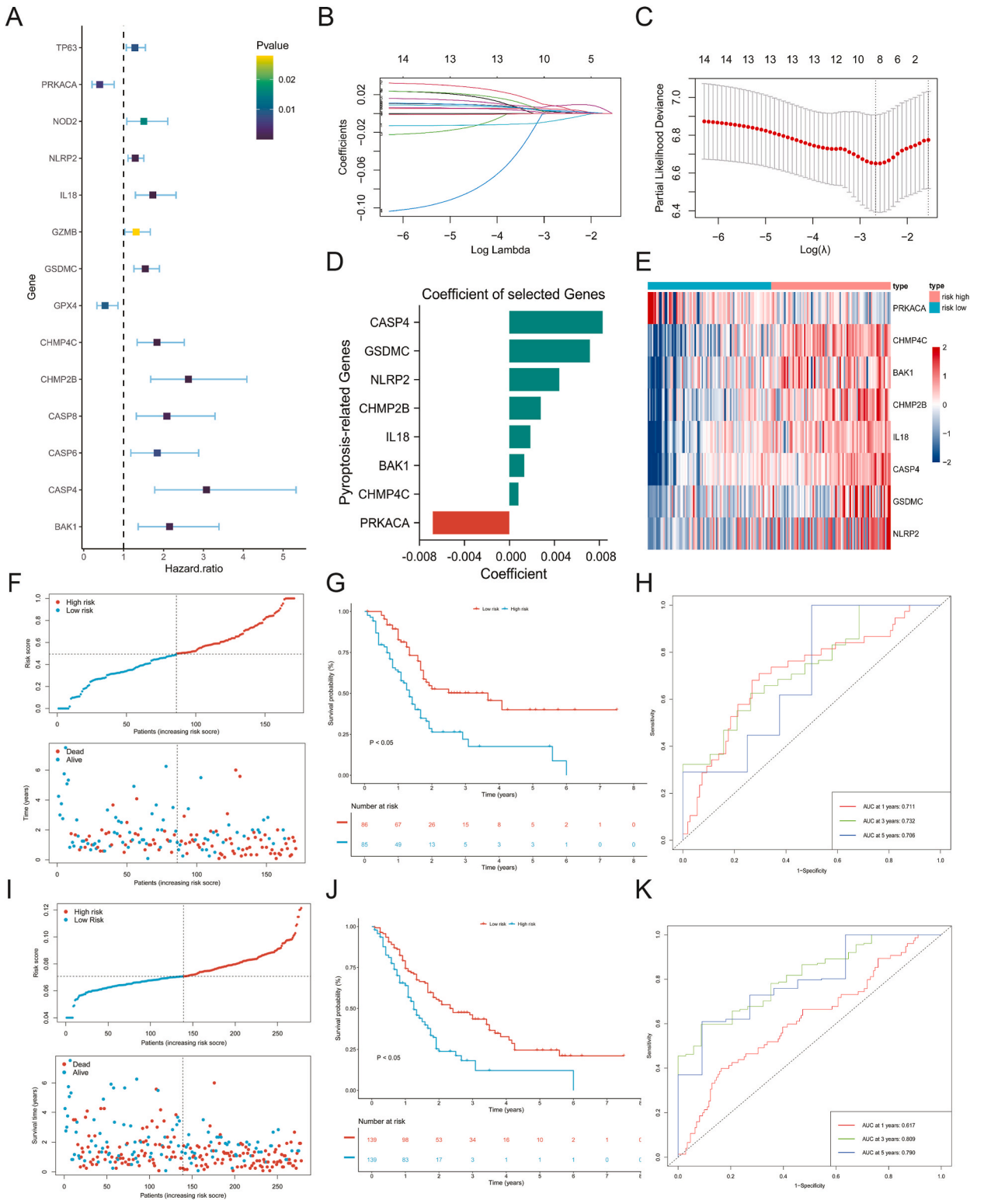

Fig. 3. | Establishment and assessment of the PRG signature in training and validation set (A) Forest map for prognostic significance of 14 DEPRGs in PAAD (B) LASSO coefficient trajectory of 14 prognostic DEPRGs (C)Tenfold cross-validation for selecting the optimal value of λ (D) The histogram exhibits the coefficients of the 8 hub prognostic genes (E) Expression heatmap of 8 signature genes in high- and low-risk subgroups (F–K) Distribution plot of survival status and time with increasing risk score; Kaplan−Meier curve for OS difference between risk subgroups; ROC curve of the PRG signature for predicting OS event in training and validation set.

2.9. Evaluation of tumor microenvironment of PRG signature

Multiple parameters associated with tumor microenvironment were calculated through the "ESTIMATE" R package [33]. The infiltration levels of 22 immunocyte subtypes in each sample were converted from the gene expression matrix using CIBERSORT algorithm [34]. The effect of PRG signature on the abudance of immunocyte subtypes and mRNA levels of key immune checkpoint genes and T cell activation genes was estimated. We also investigated the correlation of signature genes with differentially infiltrated immunocyte subtypes and key immune checkpoint genes. An external Imvigor210 cohort was used to verify the value of 8-gene signature in predicting the immunotherapy response.

2.10. Analysis of mutation spectrum

In order to compare the somatic variants between risk subgroups, mutation annotation format (MAF) and segmental copy number files of PAAD samples were retrieved from TCGA database. The waterfall chart was used to display top 20 commonly mutated genes in both high- and low-risk subgroup through "maftools" R package [35]. The copy number variation (CNV) was detected by GISTIC 2.0 database (https://www.genepattern.org/). The TMB score was calculated for every PAAD patient based on following formula: (total mutation/total covered bases) × 10^6.

2.11. Chemotherapy sensitivity analysis

To evaluate the capacity of PRG signature on predicting chemotherapeutic drug efficacy, the sensitivity of common chemotherapeutic drug in two risk subgroups were analyzed. Half maximal inhibitory concentration (IC50) is a most widely used measurement of a drug's sensitivity, which was calculated by a ridge regression model constructed by Genomics of Drug Sensitivity in Cancer (GDSC) database (www.cancerrxgene.org/) cancer cell lines drug response data and TCGA-PAAD transcriptome profiles using "pRRophetic" R package [36].

2.12. Construction and verification of predictive nomogram

Nomogram is an important approach to predict tumor prognosis. In the study, on the basis of independent clinical prognostic factors, a nomogram was constructed using "rms", "regplot" and "Hmisc" R package to evaluate the OS probability of 1-,3- and 5-year for PAAD patients. Furthermore, concordance index (C-index) was calculated to quantitatively assess accuracy of the nomogram. For determining the consistency between predicted and actual OS probabilities, calibration curve was also plotted.

3. Results

3.1. Identification of DEPRGs and pyroptosis phenotype subtypes

The whole process of our research was illustrated in Fig. 1A. An entire TCGA-GEO dataset containing 290 PAAD samples and 110 normal adjacent samples with gene expression profiles and clinical information was constructed via integrating the TCGA-PAAD and GEO datasets (GSE28735/GSE68452)(Supplementary Table 1). The principal component analysis (PCA) and box plot revealed that differences in distance and expression level between three datasets significantly reduced after removing the batch effect by "sva" R package (Fig. 1B–E). Followed by differential analysis, a total of 28 DEPRGs were extracted from the intersection of DEGs and PRGs, the mRNA level of PRGs in primary tumor samples versus normal adjacent samples was demonstrated by pheatmap (Fig. 2A). The waterfall chart for genetic mutation landscape of PRGs in PAAD was depicted, indicating TP53 as the most frequently mutated gene (Fig. 2B).

To characterize the expression pattern of PRGs in PAAD, unsupervised clustering was performed according to the expression levels of 28 DEPRGs. The CDF plot and consensus matrix heat map demonstrated that k = 3 was the optimal number of subtypes (Fig. 2C, D). Subsequently, the PAAD samples were separated into three subtypes, cluster A, cluster B and cluster C, and the independence of three subtypes was confirmed by a PCA plot (Fig. 2 E). Kaplan–Meier curve and heatmap illustrated that cluster B showing higher DEPRGs expression had a lower OS rate than that of cluster A and cluster C (Fig. 2 F; Supplementary Fig. 1A).

3.2. Establishment and assessment of a PRG signature predicting the prognosis of PAAD

First, 14 prognostic genes were recognized from 28 DEPRGs by the univariate Cox analysis, of which 2 PRGs were protective genes (HR < 1) and 12 PRGs were risk genes (HR > 1), showing in the forest map (Fig. 3A). These 14 initial candidate genes were further subjected to Lasso-penalized Cox analysis in training set, 8 hub prognostic genes (including CASP4, GSDMC, NLRP2, CHMP2B, IL18, BAK1, CHMP4C and PRKACA) were obtained based on the optimum value of λ and used to establish a PRG signature (Fig. 3 B, C). The final PRG signature based risk score was calculated as following formula: Risk score = $(0.001311101 * Exp_{BAK1}) + (0.007149094 * Exp_{GSDMC}) + (0.001863649 * Exp_{IL18}) + (0.008284412 * Exp_{CASP4}) + (0.004426405 * Exp_{NLRP2}) + (0.00278087 * Exp_{CHMP2B}) + (-0.006815925 * Exp_{PRKACA}) + (0.000804342 * Exp_{CHMP4C})$ (Fig. 3 D) Afterwards, all PAAD patients in training set (n = 176) were separated into high- and low-risk subgroup with median risk score as threshold. Expression heatmap displayed a significantly

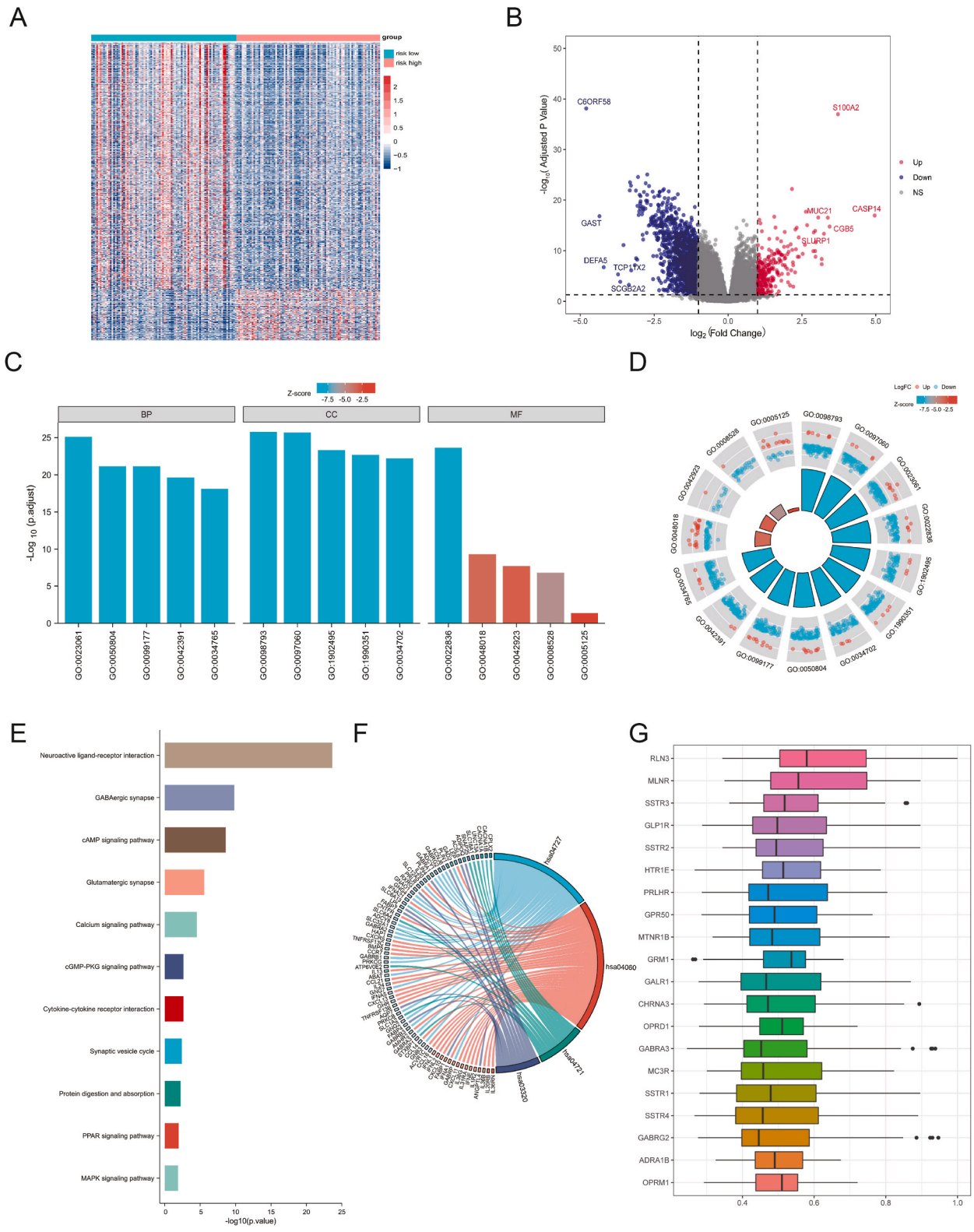

Fig. 4. | GO and KEGG enrichment analysis (A) Heatmap illustrating the expression pattern of 1198 DEGs among risk subgroups (B) Volcano map showing distribution of the 1198 DEGs (C–F) Bar diagram and circle plot showing the top significant GO terms and KEGG pathways for the DEGs between risk subgroups (G)Summary of the top 20 genes enriched in the most significant pathway in terms of functional similarity.

upregulation of GSDMC, CASP4, CHMP2B, IL18, BAK1, CHMP4C and NLRP2 in high-risk subgroup, while PRKACA was downregulated (Fig. 3 E). For verifying the prognostic prediction ability of our PRG signature, we applied the formula derived from training set to the validation set. Distributions plot depicted that the rise of risk score accompanied by an increasing dead patient number and shorter OS

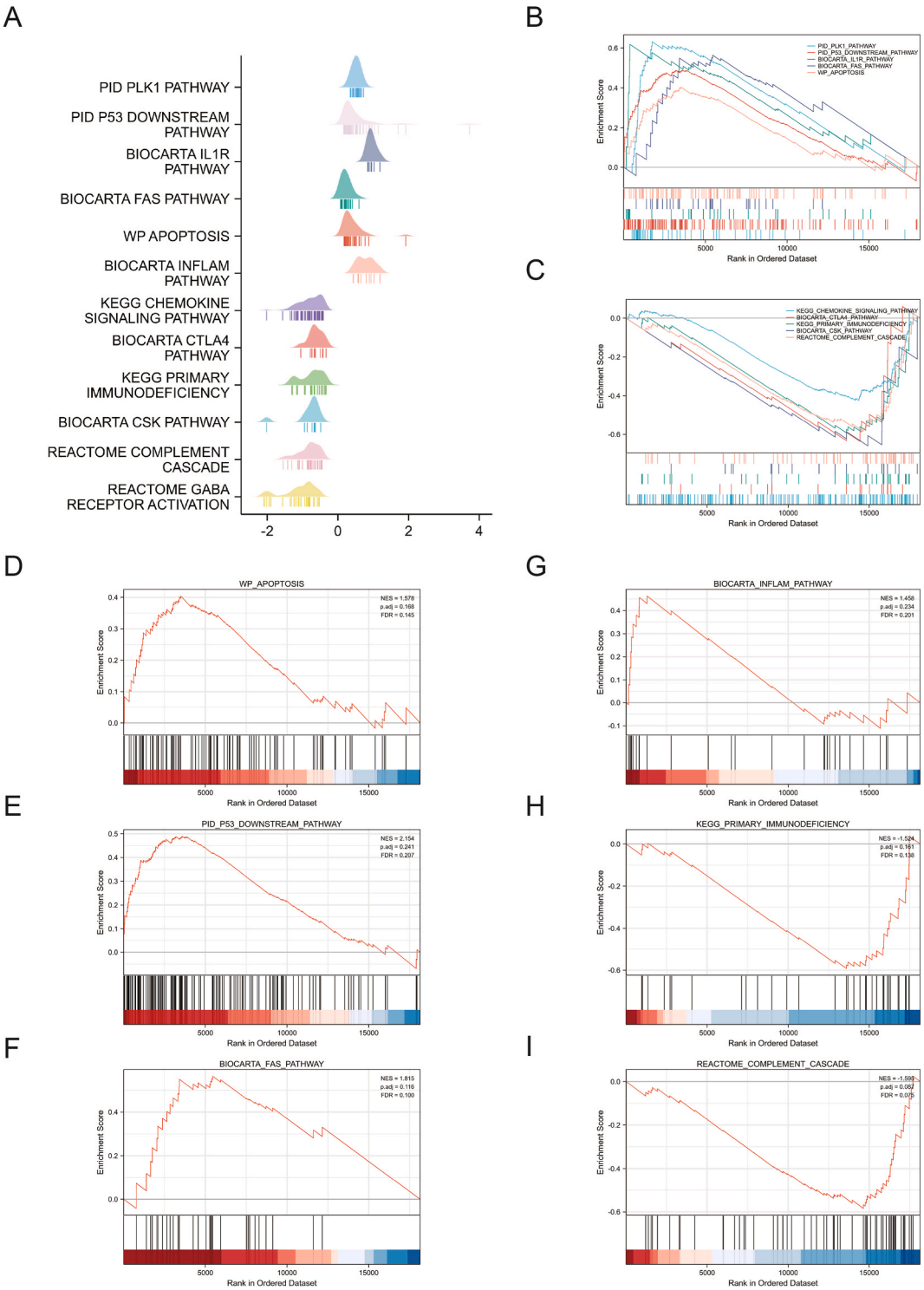

Fig. 5. | GSEA for the pathway mechanism between risk subgroups based on transcription profile (A) raincloud map for the top 12 significant pathways (B) The top 5 pathways with the highest and lowest NSE (C) The top 5 pathways with the lowest NSE in GSEA (D–I) Enrichment map showing pyroptosis related pivotal pathways.

time in both training and validation sets. Consistently, Kaplan–Meier curve proved similar result. Time-dependent ROC curve for PRG signature to predict OS event indicated that the area under the curve (AUC) was measured to be 0.711 at 1-year, 0.732 at 3-year, 0.706 at 5-year time point in training set, and 0.617, 0.809 and 0.790 for 1-year, 3-year and 5-year OS in validaton set (Fig. 3F–K).

3.3. Functional annotation of risk score related DEGs

Through differential analysis of expression profiles among risk subgroups, we obtained 1449 DEGs consisting of 1198 down-regulated and 251 up-regulated in high-risk subgroup, showing with volcano map and heatmap (Fig. 4 A, B). Subsequently, GO analysis for thses DEGs suggested the top significantly enriched terms of three GO categories highly correlated with transmembrane and *trans*-synaptic signal transduction, particularly by affecting membrane potential and neurotransmitter transmission, such as

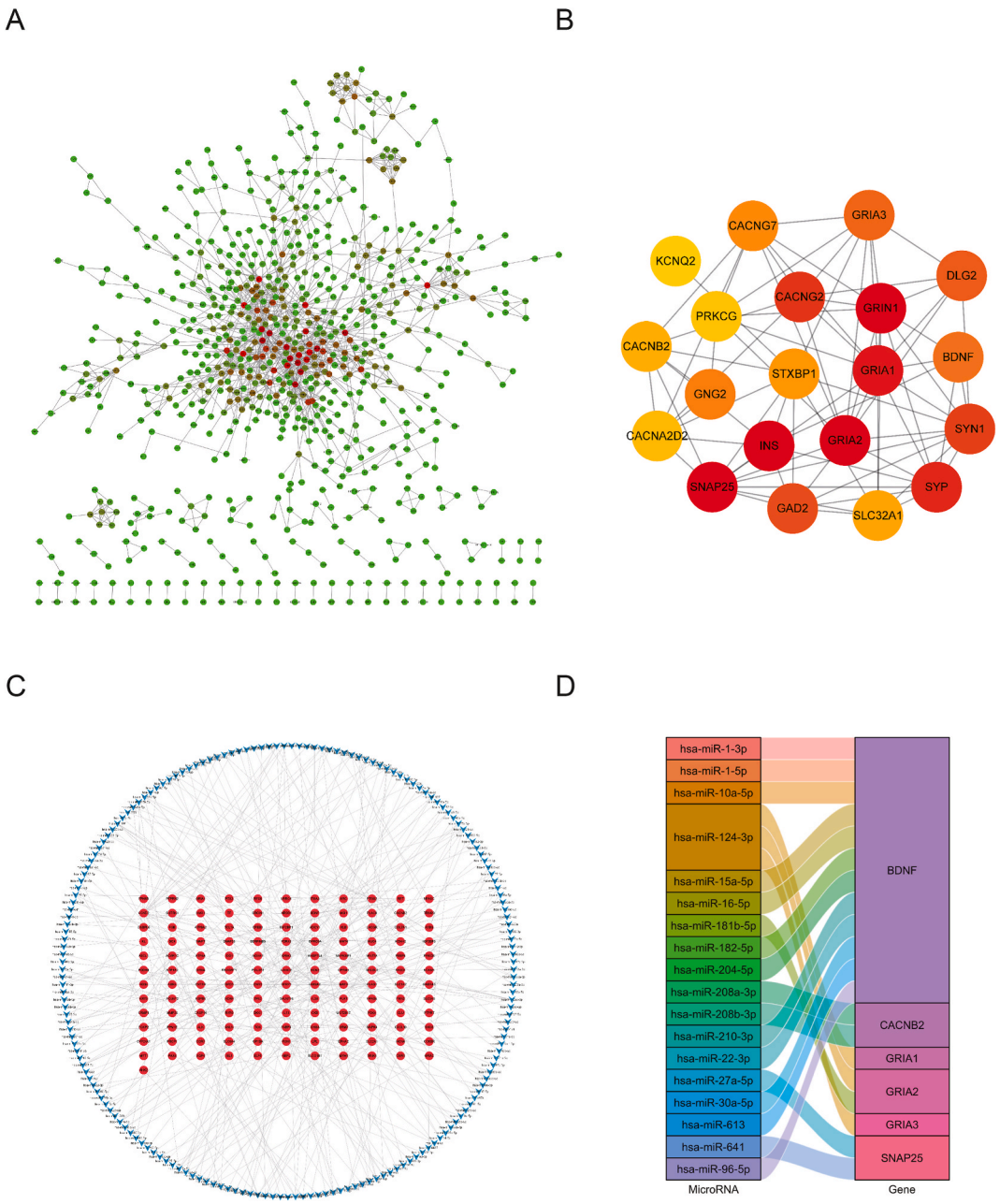

Fig. 6. | PPI and miRNA-mRNA regulatory network for DEGs comparing around risk subgroups (A) A PPI network of the interaction pairs using interaction score >0.7 as the cutoff criterion (B) The top 20 hub genes with high degrees of connectivity. The darker the red, the higher the degree (C) A miRNA-mRNA regulatory network (D) alluvial plot showing the miRNA-mRNA regulatory axes focused on the hub genes

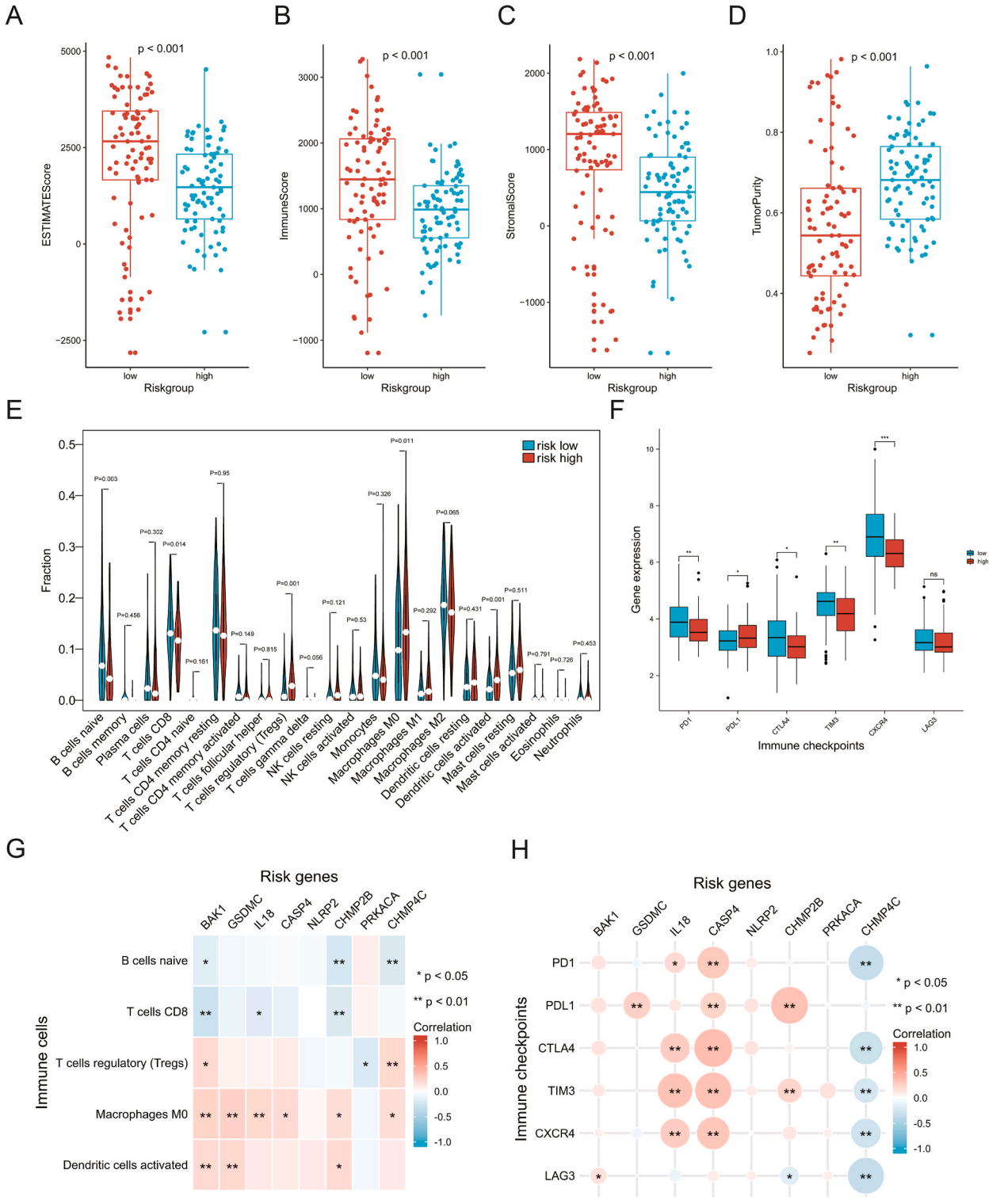

Fig. 7. | Relationship of the PRG signature with immune characterization (A–D) Distribution of immune related scores in high- and low-risk subgroup (E, F) Infiltration abundance of immunocytes and expression pattern of key immune checkpoint genes between risk subgroups (G-H) Heatmap matrix showing the correlation of signature genes with differentially infiltrated immunocytes and key immune checkpoint genes.

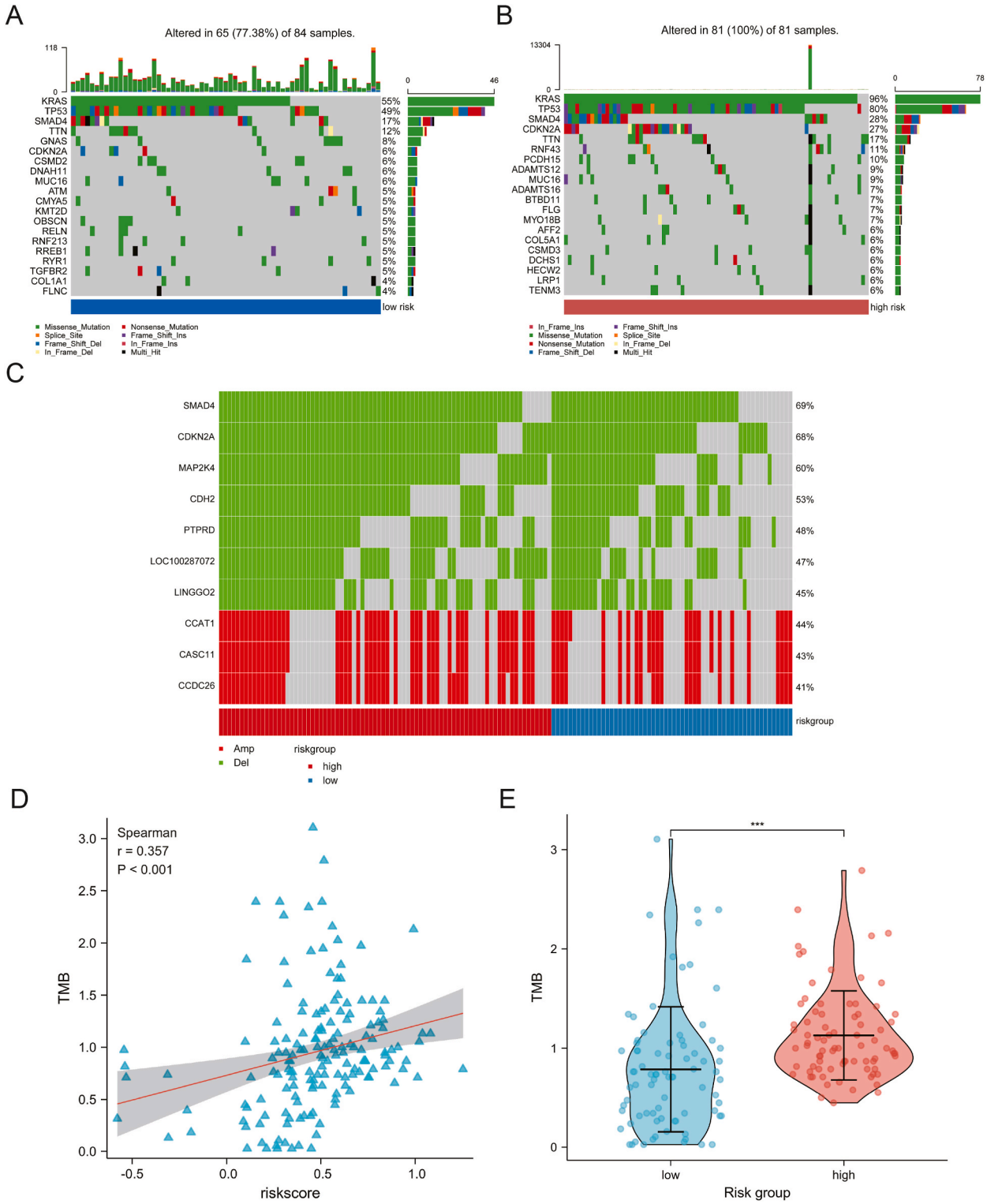

Fig. 8. | Relationship of the PRG signature with mutation(A, B) Waterfall plot showed the top 20 mutated genes in both risk subgroups (C) Integrated CNV landscape of the top 10 genes (D) Scatter plot of the correlation between TMB and risk score(E) TMB distribution among risk subgroups.

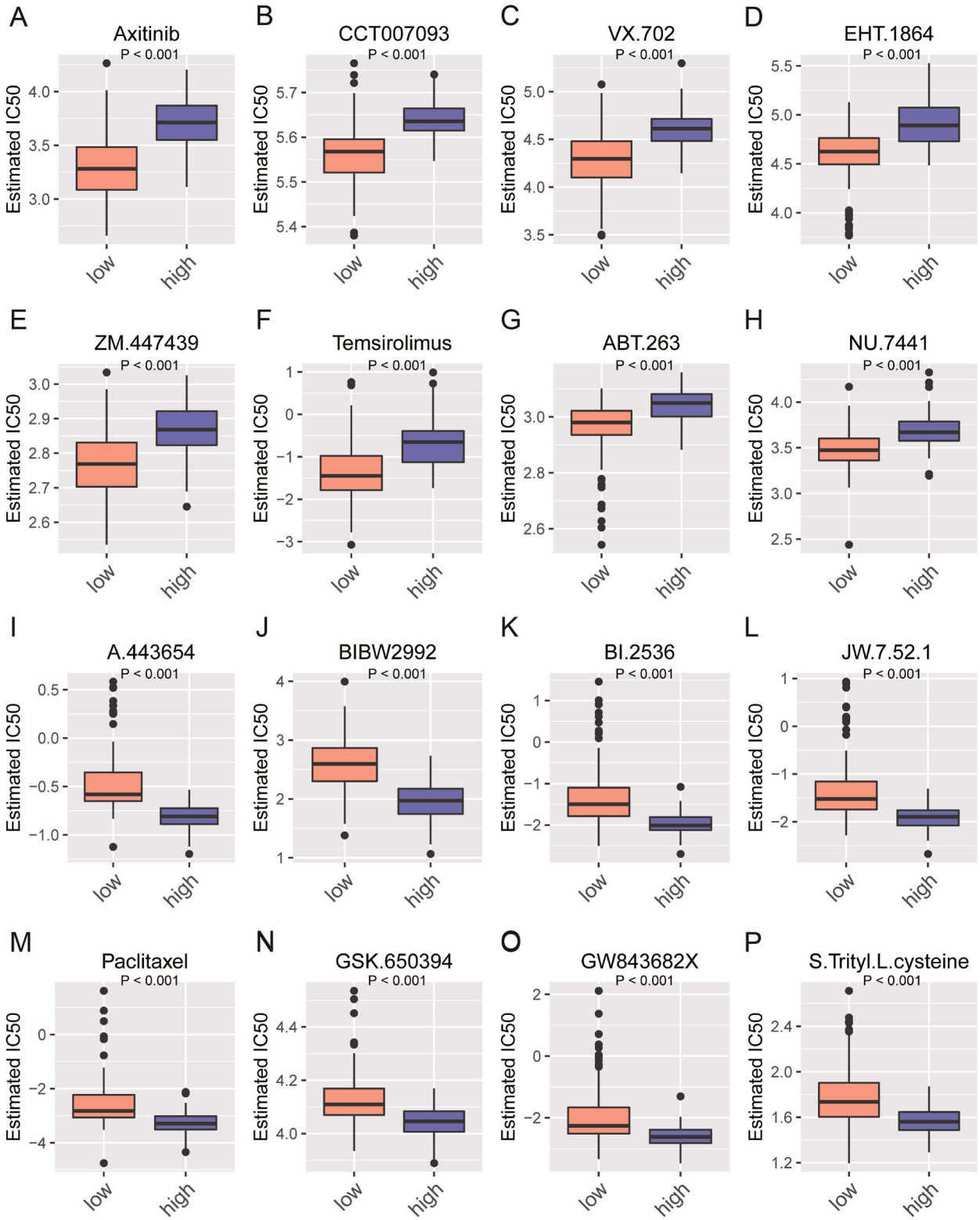

Fig. 9. | Drug sensitivity analysis of 16 common chemotherapeutic agents (A–H) Common chemotherapeutic agents with a lower IC50 value in low-risk subgroup (I–P) Common chemotherapeutic agents with a lower IC50 value in high-risk subgroup.

"regulation of ion transmembrane transport", "presynapse" and "neuropeptide binding" terms. Similarly, the KEGG pathway analysis also indicated pathways associated with signal transduction including "Neuroactive ligand-receptor interaction", "GABAergic synapse", "cAMP signaling", "Glutamatergic synapse", "Calcium signaling", "cGMP-PKG signaling", "Cytokine-cytokine receptor interaction", "Synaptic vesicle cycle", and "MAPK signaling" pathways (Fig. 4 E, F; Supplementary Tables 2 and 3). In addition, we ranked the top 20 genes enriched in the most significant pathway (hsa04080) based on the average functional similarity. The results demonstrated that RLN3 was the key role in Neuroactive ligand-receptor interaction pathway (Fig. 4G).

3.4. Gene set enrichment analysis

For further exploring the underlying pathway mechanism of PRG signature, we conducted GSEA between risk subgroups. The top 12 significant pathways were shown in the raincloud plot (Fig. 5 A; Supplementary Table 4). The top five pathways with highest normalized enrichment score (NES) were PLK1 pathway, P53 downstream pathway, IL1R pathway, FAS pathway and apoptosis (Fig. 5B). At the same time, the top five pathways with lowest NES were chemokine signaling pathway, CTLA4 pathway, primary immunodeficiency, CSK pathway and complement cascade (Fig. 5C). Among them, the pivotal pathways associated with ptroptosis process were displayed separately (Fig. 5D–I).

3.5. Construction of PPI network and miRNA-mRNA regulatory network

Base on a PPI list comprising of protein interaction pairs selected by confidence score $\geq$0.700, we built and visualized a PPI network containing 740 nodes and 1487 edges through Cytoscape software (Fig. 6A). EPC algorithm uncovered the top 20 hub genes with high degrees of connectivity in our PPI network, and interaction network between them was shown (Fig. 6B).

Furthermore, we predicted the upstream regulatory miRNAs of risk score related DEGs using "multiMiR" R package. The obtained interaction pairs of miRNA-mRNA validated by Luciferase reporter assay derived from miRTarBase database were screened to build a miRNA-mRNA regulatory network, which contained 132 mRNA and 188 miRNA, mapped by the Cytoscape software (Fig. 6C). Then, we focused on the top 20 hub genes and assessed their miRNA-target associations, a total of 6 hub gens including BDNF, CACNB2, GRIA1, GRIA2, GRIA3, SNAP25, and their corresponding upstream regulatory miRNAs were displayed in the alluvial plot (Fig. 6 D; Supplementary Table 5)

3.6. TME analysis between risk subgroups

Previous findings revealed by GSEA indicated that our PRG signature was highly correlated with the immunity inflammation pathways, thus we investigated the impact of PRG signature on TME. Through ESTIMATE algorithm, we discovered that patients in high-risk subgroup had lower ESTIMATE score, immune score, and stromal score, as well as higher tumor purity than low-risk subgroup (Fig. 7A–D).For the infiltrating level of different immunocytes derived from CIBERSORT algorithm, significantly higher abundance of regulatory T cells(Tregs), M0 Macrophages, activated Dendritic cells (DCs), and lower abundance of naïve B cells,CD8+ T cells was observed in high-risk subgroup (Fig. 7 E).The correlations between immunocytes were displayed (Supplementary Fig. 1B).

We also studied the expression levels of key immune checkpoint genes which had become a vital biomarker for the selection of immunotherapy. Most of immune checkpoint genes (except PDL1) and T cell activation genes (except GZMB and IFNG) were highly expressed in low-risk subgroup (Fig. 7 F, Supplementary Fig. 2C). To validate these findings above, we conducted spearman correlation analysis of signature genes with differentially infiltrated immunocytes and key immune checkpoint genes, which revealed that the expression of most signature genes had a positive correlation with Tregs, M0 Macrophages, activated DCs, and a negtive correlation with naïve B cells and $CD8^+$ T cells(Fig. 7 G). Meanwhile, significant correlation was also observed with key immune checkpoint genes (Fig. 7H).In IMvigor210 cohort, patients with low-risk group stratified by the 8-gene signature exhibited a significantly better prognosis.In addition, we discovered that patients who responded to ICI therapy had a slightly lower risk score than those who did not respond(Supplementary Figs. 2A and B).

3.7. The PRG signature and mutation landscape

The mutation profiles of PAAD samples from TCGA cohort were summarized, we displayed the mutation frequency and type of the top 20 significantly mutated genes in both risk subgroups respectively (Fig. 8 A, B). Overall, the high-risk subgroup exhibited slightly higher somatic mutation frequency than that low-risk subgroup. Notably, KRAS, TP53, SMAD4, TTN, CDKN2A and MUC16 were common genes in the top 10 most frequently mutated genes of both risk subgroups. Then an integrated landscape showed the distribution of CNVs among risk subgroups (Fig. 8C). In the top 10 genes with highest CNV rate, CCAT1, CASC11, and CCDC26 were copy number amplified genes, which were known as proto-oncogenes.While SMAD4, CDKN2A, MAP2K4, CDH2, PTRRD, LOC100287072 and LINGO2 were copy number deleted genes, which were generally considered as anti-oncogenes. In addition, the high-risk subgroup had a relatively higher TMB, consistency with correlation between TMB and risk score (Fig. 8D and E). However, the microsatellite instability (MSI) did not differ significantly among risk subgroups (Supplementary Figs. 1C and D).

3.8. Evaluation of chemosensitivity by the PRG signature

We assesed the predictive effect of the PRG signature on the efficacy of conventional chemotherapy drugs using the pRRophetic

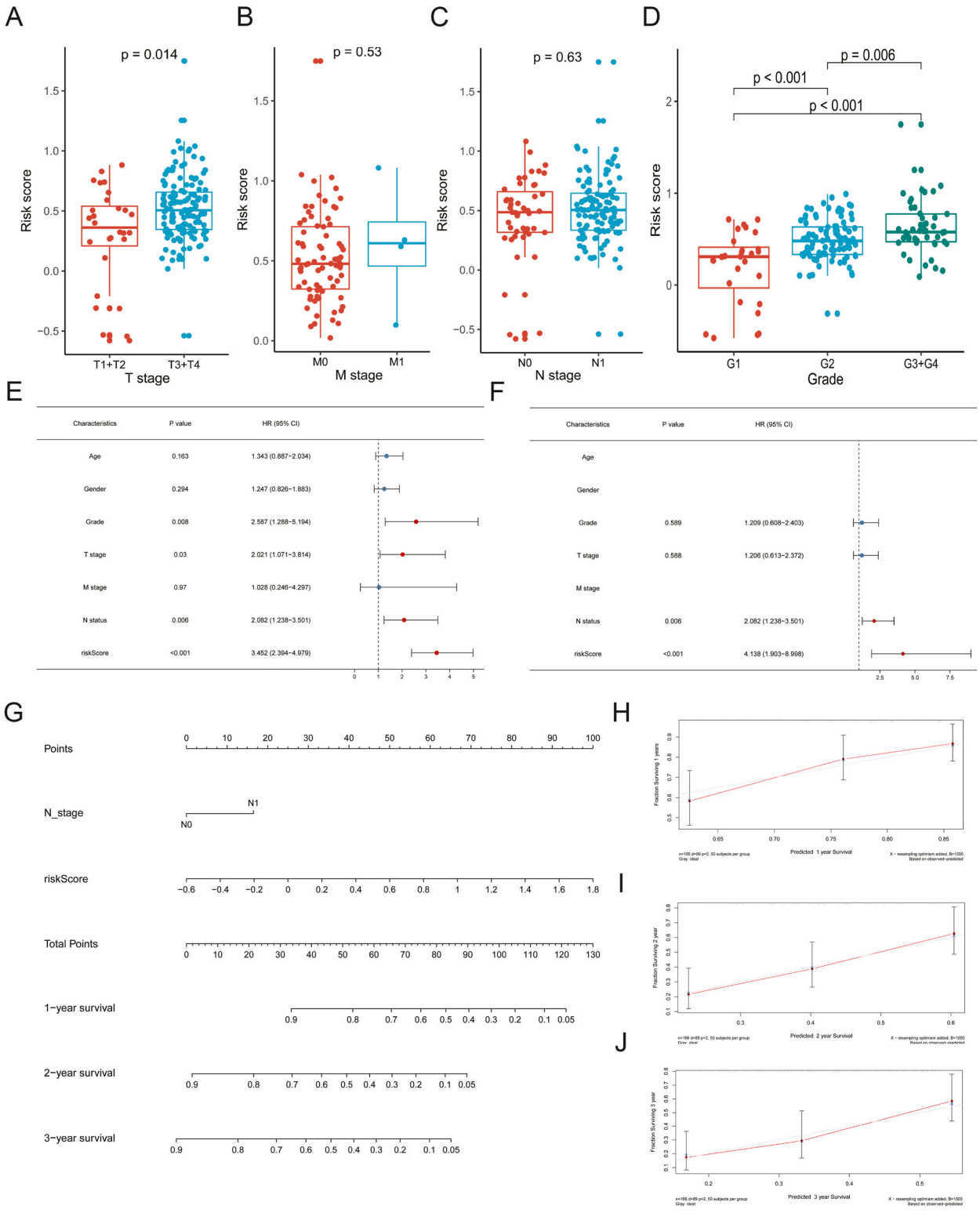

Fig. 10. | Construction of a PRG signature-based nomogram for clinical application(A-D) Distribution of risk score between diverse clinicopathologic features (E,F) Forest plot showing the prognostic significance of multiple clinical parameters (G-J)The PRG signature-based nomogram and validated calibration curves for 1-, 2- and 3-year OS prediction perfomance

algorithm. Our study demonstrated that the IC50 levels of Axitinib, CCT007093, VX.702, EHT.1864, ZM.447439, Temsirolimus, ABT.263 and NU.7441 were markedly lower in low-risk subgroup, and the IC50 levels of A.443654, BIBW2992, BI.2536, JW.7.52.1, Paclitaxel, GSK.650394, GW843682X and S-Trityl-L-cysteine were opposite (Fig. 9A–P). Our results suggested that the PRG signature was an efficient tool for selection of clinical Chemotherapy regimen in PAAD patients.

3.9. Development of a PRG signature-based nomogram for individual prognostic prediction

We firstly investigated the distribution of risk score between different clinicopathologic features (Fig. 10 A-D; Supplementary Table 6). Significant differences were observed in T stage and grade (Fig. 10 A, D). Univariate and multivariate analysis illustrated that only N stage and risk score were considered as independent prognostic factors linked with OS (Fig. 10E and F). Ultimately, we constructed a new nomogram combined with N stage and risk score to evaluate the OS probability for PAAD patients (Fig. 10 G). The C-indexof our 0.66, and calibration curves demonstrated that the predicted OS probabilities were considerable agreement with actual OS probabilities (Fig. 10H–J).

4. Discussion

It has become increasingly appreciated that PAAD is a highly heterogeneous disease. The genetic heterogeneity between individual tumors has been an obstacle in PAAD characterization and considered as a crucial cause of discrepancy in prognosis and varying degree of resistance to current approved therapeutic strategies [37,38]. With the widespread application of high-throughput sequencing, there is a deeper understanding of underlying molecular mechanism that causes PAAD intratumor heterogeneity and the search for novel therapeutic targets. In addition, a precise clinically relevant molecular subtype classification system could be developed utilizing the genetic and transcriptomic information to predict survival outcome and therapeutic response of PAAD patients.

Cell death is a process of fundamental importance to tumor pathogenesis.The progression and treatment response of tumor are affected by a wide variety of cell death forms, such as cuproptosis, pyroptosis and anoikis.Recently, the prognostic value of PRGs has attracted more attention in malignant tumors. Shi et al. verified that colorectal cancer (CRC) patients with elevated NLRP3 expression had a worse prognosis [39]. David Sarrió et al. reported that the GSDMB promoted the invasive and migratory phenotype of breast carcinoma and could be considered as a new potential prognostic indicator [40]. However, the predictive ability depending on a single gene is usually unreliable because a single gene could participate in a variety of biological processes and be regulated by multiple signal pathways. The construction of a polygene risk signature according to the expression characteristic of core regulatory factors that involved in the same biological function is of great significance to elevate the prediction accuracy. In our study, we systematically analyzed the transcriptional level, somatic variant and prognostic relevance of 46 PRGs. As expected, although these PRGs were conservative and stable at genetic level, approximate 60 % (28/46) of them were identified as DEGs between PAAD and normal adjacent tissue. While univariate analysis revealed that 50 % (14/28) DEPRGs were associated with OS, implying that pyroptosis might be potential prognostic biomarkers for PAAD. To gain insight into the prognostic role of PRGs in PAAD, a 8-gene signature consisting of CASP4, GSDMC, NLRP2, CHMP2B, IL18, BAK1, CHMP4C and PRKACA was established, which could accurately predict survival outcome of PAAD.

Among the risk genes in our PRG signature, most of them except PRKACA were adverse prognostic factor. CASP4 was a key component of non-canonical pyroptosis pathway, it could participate in innate immune response to defend against infection of pathogenic bacteria [41]. In the progress of cancer, Giuliana Papoff et al. indicated that the down-regulation of CASP4 could lead to an impairment in migratory and cell-matrix adhesion behavior of epithelial cancer cell lines through actin remodeling [42].CHMP4C was a member of charged multivesicular body protein (CHMP) family, it involved in composition of the endosomal sorting complex required for transport (ESCRT) which mediated the damage repair and blebbing of plasma membrane during pyroptosis [43–45].Some researchers suggested that CHMP4C overexpression was linked to poor prognosis in patients with lung squamous carcinogenesis (LUSC) and cervical carcinoma (CC) [9,10],whereas depletion of CHMP4C will result in S-phase arrest of tumor cells, thus inhibiting tumor growth. The upregulated mRNA level of CASP4 and CHMP4C in PAAD patients with poor prognosis were consistent with the results of Chen's report, the research also revealed that the knockdown of CASP4 and CHMP4C obviously inhibited the invasion and migration of PANC-1 cells at experiment level [46].

CHMP2B was another member of CHMP family, which participate together with CHMP4C in composition of the ESCRT-III to constrict and stabilize membrane structures in membrane remodeling processes [47].Unfortunately, the basic study of CHMP2B related to tumor prognosis was rare. GSDMC was a member of gasdermin protein family, the cleavage of GSDMC by activated caspase-8 could induce pyroptosis in HeLa cervical carcinoma cells treated with α-ketoglutarate (α-KG) [48].GSDMC was generally considered as a risk factor in several tumor types such as kidney renal clear cell carcinoma(KIRC) and LUAD [15,49,50], GSDMC was also an oncogene in our study. In contrast, GSDMC exhibited to be a tumor suppressor in gastric cancer [51], demonstrating that the actual functional role of GSDMC might exert tissue specifically.IL-18 was one of the downstream productions during pyroptosis process, which could increase the NF-κB activity in pancreatic cancer cells and be confirmed as a predictor of poor prognosis [52].NLRP2 belonged to NLRs family, which was a crucial type of innate immune sensor. The NLRP2 overexpression was confirmed to play an unrecognized role in regulating proinflammatory responses [53]. BAK1 was a critical apoptosis regulator, Jinyu Zhu's study validated that knockdown of BAK1 significantly suppressed hepatocellular carcinoma cells proliferation and promoted apoptosis [54]. Kohsuke Tsuchiya reported that under certein circumstances pyroptosis could be switched to apoptosis, so it was speculated that the BAK1 could influence pyroptosis through modulating apoptosis process [55].

As the only protective prognostic factor, PRKACA was also associated with apoptosis. PRKACA was known to encode the main

catalytic subunit of protein kinase A (PKA) that led to activation of cAMP/PKA pathway which has been found to promote apoptosis of pancreatic cancer cells [56].

GO and KEGG analysis revealed that the transcription discrepancy between risk subgroups mainly involved in complicated signal transduction, which might be mediated by cascade reaction of inflammasome signaling complex during pyroptosis process. The PPI network revealed that the top 20 hub genes mainly belonged to the ionotropic glutamate receptor superfamily and synapsin gene family which were also associated with signal transduction. The GSEA results showed that high-risk subgroup primarily focused on programmed cell death and malignant progression related pathways such as apoptosis pathway, PLK1 pathway and IL-1R pathway. The appearance of apoptosis pathway was not surprisingly, Gurung et al. have discovered that core components of apoptosis-inducing caspase cascade including caspase-8 and FADD could regulate NLRP3 inflammasome signaling as apical mediators, suggesting a co-regulation and crosstalk between apoptosis and pyroptosis pathway [57]. The PLK1 pathway and IL-1R pathway were both associated with poor patient outcome [58].PLK1 could trigger tumor cell proliferation through accelerating S-phase progression and promoting mitotic entry by means of activating the cyclin B/cdc2 complex [59].For IL-1R pathway, as one of the pyroptosis production downstream pathways, growing evidence demonstrated that it could induce the generation of proteases and cytokines that significantly change extracellular matrix [60].These upregulated molecules were also linked to recruitment of innate immunocytes such as macrophages, which will secrete angiogenic growth factors that enhance the oxygen and nutrients supply and vascular permeability, thus helping tumor cells disrupt the endothelial barrier and infiltrate into deep tissues [61]. While low-risk subgroup was mainly in relation to immune and inflammatory response related pathways such as CTLA4 pathway, chemokine signaling and complement cascade pathway, which might be a substantial evidence for the mmunologically active state of low-risk subgroup.

In recent years, TME is a spotlight in oncology [62]. Pyroptosis could serve as a link between immune system and tumor immunity. The traditional brief concluded that the patients with high immune activity and low tumor purity exhibited a better prognosis [63], the association between TME and PRG signature in our research was consistent with it.CD8+ T cell had been found in proximity to cancer cells and known as a critical anti-tumor immune cell due its cytotoxicity, some researchers reported that lower $CD8^+$ T cell infiltration represented an unfavorable outcome in pancreatic cancer [64,65], and our results confirmed this finding. Effector $CD8^+$ T cell with activated cytotoxic phenotype eventually paly a role in clearance of tumor cells. Recognizing the activation status of $CD8^+$ T cell is of great significance for understanding the antitumor activity of TME.As previous study reported, a T cell activation gene set including NKG7, CCL4, CST7, PRF1, GZMA, GZMB, IFNG and CCL3 which mainly involved the secretion of cytotoxic cytokines has been defined to differentiate cell subsets and heterogeneity of activation status within $CD8^+$ T cell [66,67]We discovered that these $CD8^+$ T cell activation markers were almost highly expressed in low risk group, implying an increased activation status of $CD8^+$ T cell in low risk group.Interestingly, these cytotoxic markers exhibited a similar expression pattern with inhibitory checkpoint molecules in two risk subgroups, which consistent with a "activation-dependent exhaustion expression programme" that has previously been described [68]. Unexpectedly, the infiltration of activated dendritic cell was higher in high-risk subgroup. Dendritic cells are predominant antigen-presenting cells that act a critical role in promoting anti-tumor CD8+T cell immunity [69]. It could be presumed that higher infiltration level of dendritic cell was correlated with high TMB level in high-risk subgroup, and there was an impairment in function of dendritic cell to recruit and stimulate CD8+T cell. The insufficient CD8+T cell might be mediated by the regulatory T cells (Tregs) which was more abundant in high-risk group, an earlier study showed that Tregs could downregulate the level of co-stimulatory molecules in dendritic cells as well as limit the interaction with conventional T cells, thus impairing the DC immunogenicity and alleviating CD8+T cell activation [70]. Notably, MUC16 exhibited higher mutation frequency in high-risk group, which conflicted with the conclusion that MUC16 mutation was associated with longer survival time in PAAD [71]. Elevated MUC16 mutation might contribute to increased neoantigen formation and thus enhancing anti-tumor immune response [72]. However, other factors such as the dysfunction of CD8+T cell and other genetic alterations might counteract the potential beneficial effects of MUC16 mutation. Therefore,it is worthy exploring the effect of somatic mutation in tumor microenvironment, including recruitment and activation of immune cells, and potential impact on immunotherapy response.

Immune checkpoint inhibitors(ICIs) known as an important immunotherapy option have showed promising therapeutic effects in various solid tumors including melanoma, bladder as well as renal cancer [73].However, this novel therapeutic approach failed to elicit response in most of PAAD patients, and tumor genotyping system that identify patients more likely to benefit from ICIs treatment was limited. Our research revealed that patients in low-risk group exhibited higher expression of ICIs-related moleculars such as PD-1, CTLA-4, TIM-3 and CXCR4, and it has been reported that the expression level of ICIs-related moleculars can serve as a biomarker to forecast the efficacy of ICIs therapy [23]. PD-1 is expressed on a variety of immune cells especially on activated T cells, and also marked as an indicator for activation of $CD8^+$ T-cell [74], which consistent with the finding that higher expression of PD-1 indicated better prognosis. PD-L1 known as an indicator of tumor burden was the most important ligand of PD-1, exhibited opposite expression pattern. The relation of PD-L1 with poor prognosis in PAAD had been conformed by other academics. In Loos M et al.'s study [75], patients with high PD-L1 expression only had a 10-month median survival time compared to those with low PD-L1 expression, who had a 24-month median survival time.Similar conclusion was also reported by Birnbaum DJ et al. with the evidence of lymphocyte exhaustion mediated by PD-L1 [76].A newly published study involving tumor-stroma interplay found that high local abundance of macrophage usually accompanied with strong PD-L1 staining in tumoral lesions of PAAD , but the cytotoxic phenotype of $CD8^+$ T cells co-cultured in PAAD macrophage spheroids was not enhanced by the ICIs treatment [77].So it could be speculated that the high-risk group with high expression of PD-L1 which might be partially mediated by higher abundance of macrophage didn't respond to ICIs treatment. Overall, we discovered that our PRG signature was a reference toolr to recognize PAAD patients who might be more sensitive to ICIs.

We also predicted potential response to conventional chemotherapeutic agents in high-risk versus low-risk group using GDSC database and pRRophetic algorithm. The cornerstone of PAAD treatment is still systemic chemotherapy. As a crucial agent of first-line chemotherapy against pancreatic cancer, it has been reported paclitaxel could induce pyroptosis in various types of cancer [78,79]. In

our study, paclitaxel exhibited potential higher sensitivity in high-risk group, which might be mediated by the function of PRGs in regulating cell proliferation and apoptosis [80,81]. Some researches reported that the programed death pattern of tumor cells expressing high levels of PRGs such as GSDME and GSDMC coud be swiched from apoptosis to pyroptosis induced by chemotherapy, leading to a extensive inflammatory response [17,82]. BI 2536, a novel small molecule inhibitor, was another chemotherapeutic agent exhibited higher sensitivity in high-risk group. Jianting Huo et al. reported that the BI 2536 exerted antitumoral effect through inducing pyroptosis and accumulation of $CD8^+$ T cells [83],which was less infiltrating in high-risk group. Future research should focus on exploring the precise mechanism by which the PRGs regulate sensitivity of chemotherapeutic agents.

It must be acknowledged that there are several shortcomings in our research. Firstly, as a retrospective analysis, both training and validation datasets included in our research were retrieved from public databases, thus prospective clinical cohort is needed to validate the prediction performance of the risk signature. Secondly, some crucial clinical information especially response to conventional chemotherapy and immunotherapy were not available in our datasets, which might be helpful to understand whether the PRG signature is a reliable predictive factor of treatment response. Last but not least, the molecular mechanism how PRGs in the risk signature regulate the precise process of PAAD remains unclear, so further fundamental experiments including cellular and animal models are necessary to explore it. We hope that the aforementioned limitations could be solved in the future.

In conclusion, we developed a novel PRG signature and preliminarily assessed its efficacy in foretelling the outcome of PAAD patients. We also investigated the guiding significance of the PRG signature for chemotherapy and immunotherapy response. Future studies on the prospective randomized clinical trials and specific mechanisms of these pyroptosis related risk genes will be clinically helpful.

Data availability statement

The data associated with our study are publicly available in [The Cancer Genome Atlas Database; Gene Expression Omnibus; IMvigor210CoreBiologies package], accession number[TCGA-PAAD; GSE62452; GSE28735; IMvigor 210]

CRediT authorship contribution statement

Jieting Zhou: Data curation, Formal analysis, Visualization, Writing – original draft, Writing – review & editing, Investigation, Methodology. **Jian Fan:** Conceptualization, Supervision, Writing – review & editing. **Binxiao Li:** Data curation, Software, Writing – original draft. **Jiayu Sun:** Data curation, Software, Writing – original draft. **Jingchao Wang:** Resources, Software, Visualization.

Declaration of competing interest

The authors declare that they have no known competing financial interests or personal relationships that could have appeared to influence the work reported in this paper.

Appendix A. Supplementary data

Supplementary data to this article can be found online at https://doi.org/10.1016/j.heliyon.2023.e23004.

References

[1] H. Ying, P. Dey, W. Yao, A.C. Kimmelman, G.F. Draetta, A. Maitra, et al., Genetics and biology of pancreatic ductal adenocarcinoma[J], Genes Dev. 30 (4) (2016) 355–385.
[2] P. Rawla, T. Sunkara, V. Gaduputi, Epidemiology of pancreatic cancer: global trends, etiology and risk factors[J], World J. Oncol. 10 (1) (2019) 10–27.
[3] L. Rahib, B.D. Smith, R. Aizenberg, A.B. Rosenzweig, J.M. Fleshman, L.M. Matrisian, Projecting cancer incidence and deaths to 2030: the unexpected burden of thyroid, liver, and pancreas cancers in the United States[J], Cancer Res. 74 (11) (2014) 2913–2921.
[4] O. Strobel, J. Neoptolemos, D. Jager, M.W. Buchler, Optimizing the outcomes of pancreatic cancer surgery[J], Nat. Rev. Clin. Oncol. 16 (1) (2019) 11–26.
[5] H. Okasha, S. Elkholy, R. El-Sayed, M.N. Wifi, M. El-Nady, W. El-Nabawi, et al., Real time endoscopic ultrasound elastography and strain ratio in the diagnosis of solid pancreatic lesions[J], World J. Gastroenterol. 23 (32) (2017) 5962–5968.
[6] T.B. Karasic, M.H. O'Hara, A. Loaiza-Bonilla, K.A. Reiss, U.R. Teitelbaum, E. Borazanci, et al., Effect of gemcitabine and nab-paclitaxel with or without hydroxychloroquine on patients with advanced pancreatic cancer: a phase 2 randomized clinical trial[J], JAMA Oncol. 5 (7) (2019) 993–998.
[7] J.P. Neoptolemos, J. Kleeff, P. Michl, E. Costello, W. Greenhalf, D.H. Palmer, Therapeutic developments in pancreatic cancer: current and future perspectives[J], Nat. Rev. Gastroenterol. Hepatol. 15 (6) (2018) 333–348.
[8] D. Delitto, S.M. Wallet, S.J. Hughes, Targeting tumor tolerance: a new hope for pancreatic cancer therapy?[J], Pharmacol. Ther. 166 (2016) 9–29.
[9] T. Bergsbaken, S.L. Fink, B.T. Cookson, Pyroptosis: host cell death and inflammation[J], Nat. Rev. Microbiol. 7 (2) (2009) 99–109.
[10] X. Liu, Z. Zhang, J. Ruan, Y. Pan, V.G. Magupalli, H. Wu, et al., Inflammasome-activated gasdermin D causes pyroptosis by forming membrane pores[J], Nature 535 (7610) (2016) 153–158.
[11] D. Frank, J.E. Vince, Pyroptosis versus necroptosis: similarities, differences, and crosstalk, Cell Death Differ. 26 (1) (2019) 99–114.
[12] P. Broz, P. Pelegrin, F. Shao, The gasdermins, a protein family executing cell death and inflammation[J], Nat. Rev. Immunol. 20 (3) (2020) 143–157.
[13] D. Tang, R. Kang, T.V. Berghe, P. Vandenabeele, G. Kroemer, The molecular machinery of regulated cell death[J], Cell Res. 29 (5) (2019) 347–364.
[14] J. Shi, Y. Zhao, Y. Wang, W. Gao, J. Ding, P. Li, et al., Inflammatory caspases are innate immune receptors for intracellular LPS[J], Nature 514 (7521) (2014) 187–192.
[15] S. Feng, D. Fox, S.M. Man, Mechanisms of gasdermin family members in inflammasome signaling and cell death[J], J. Mol. Biol. 430 (18 Pt B) (2018) 3068–3080.

[16] J. Shi, Y. Zhao, K. Wang, X. Shi, Y. Wang, H. Huang, et al., Cleavage of GSDMD by inflammatory caspases determines pyroptotic cell death[J], Nature 526 (7575) (2015) 660–665.
[17] Y. Wang, W. Gao, X. Shi, J. Ding, W. Liu, H. He, et al., Chemotherapy drugs induce pyroptosis through caspase-3 cleavage of a gasdermin[J], Nature 547 (7661) (2017) 99–103.
[18] Z. Zhou, H. He, K. Wang, X. Shi, Y. Wang, Y. Su, et al., Granzyme A from cytotoxic lymphocytes cleaves GSDMB to trigger pyroptosis in target cells[J], Science (6494) (2020) 368.
[19] Y. Tan, Q. Chen, X. Li, Z. Zeng, W. Xiong, G. Li, et al., Pyroptosis: a new paradigm of cell death for fighting against cancer[J], J. Exp. Clin. Cancer Res. 40 (1) (2021) 153.
[20] Y.Y. Wang, X.L. Liu, R. Zhao, Induction of pyroptosis and its implications in cancer management[J], Front. Oncol. 9 (2019) 971.
[21] W. Lin, Y. Chen, B. Wu, Y. Chen, Z. Li, Identification of the pyroptosis-related prognostic gene signature and the associated regulation axis in lung adenocarcinoma[J], Cell Death Dis. 7 (1) (2021) 161.
[22] M. Deng, S. Sun, R. Zhao, R. Guan, Z. Zhang, S. Li, et al., The pyroptosis-related gene signature predicts prognosis and indicates immune activity in hepatocellular carcinoma[J], Mol. Med. 28 (1) (2022) 16.
[23] Z. Zhou, J. Xu, N. Huang, J. Tang, P. Ma, Y. Cheng, A pyroptosis-related gene signature associated with prognosis and tumor immune microenvironment in gliomas[J], Int. J. Gen. Med. 15 (2022) 4753–4769.
[24] J.T. Leek, W.E. Johnson, H.S. Parker, A.E. Jaffe, J.D. Storey, The sva package for removing batch effects and other unwanted variation in high-throughput experiments[J], Bioinformatics 28 (6) (2012) 882–883.
[25] M.E. Ritchie, B. Phipson, D. Wu, Y. Hu, C.W. Law, W. Shi, et al., Limma powers differential expression analyses for RNA-sequencing and microarray studies[J], Nucleic Acids Res. 43 (7) (2015) e47.
[26] M.D. Wilkerson, D.N. Hayes, ConsensusClusterPlus: a class discovery tool with confidence assessments and item tracking[J], Bioinformatics 26 (12) (2010) 1572–1573.
[27] Q. Yuan, W. Zhang, W. Shang, Identification and validation of a prognostic risk-scoring model based on sphingolipid metabolism-associated cluster in colon adenocarcinoma[J], Front. Endocrinol. 13 (2022), 1045167.
[28] Q. Yuan, J. Ren, X. Chen, Y. Dong, D. Shang, Contributions and prognostic performances of m7G RNA regulators in pancreatic adenocarcinoma[J], Chin. Med. J. 135 (17) (2022) 2101–2103.
[29] Q. Yuan, J. Ren, Z. Wang, L. Ji, D. Deng, D. Shang, Identification of the real hub gene and construction of a novel prognostic signature for pancreatic adenocarcinoma based on the weighted gene Co-expression network analysis and least absolute shrinkage and selection operator algorithms[J], Front. Genet. 12 (2021), 692953.
[30] G. Yu, L.G. Wang, Y. Han, Q.Y. He, clusterProfiler: an R package for comparing biological themes among gene clusters[J], OMICS 16 (5) (2012) 284–287.
[31] G. Yu, F. Li, Y. Qin, X. Bo, Y. Wu, S. Wang, GOSemSim: an R package for measuring semantic similarity among GO terms and gene products[J], Bioinformatics 26 (7) (2010) 976–978.
[32] Y. Ru, K.J. Kechris, B. Tabakoff, P. Hoffman, R.A. Radcliffe, R. Bowler, et al., The multiMiR R package and database: integration of microRNA-target interactions along with their disease and drug associations[J], Nucleic Acids Res. 42 (17) (2014) e133.
[33] K. Yoshihara, M. Shahmoradgoli, E. Martinez, R. Vegesna, H. Kim, W. Torres-Garcia, et al., Inferring tumour purity and stromal and immune cell admixture from expression data[J], Nat. Commun. 4 (2013) 2612.
[34] A.M. Newman, C.L. Liu, M.R. Green, A.J. Gentles, W. Feng, Y. Xu, et al., Robust enumeration of cell subsets from tissue expression profiles[J], Nat. Methods 12 (5) (2015) 453–457.
[35] A. Mayakonda, D.C. Lin, Y. Assenov, C. Plass, H.P. Koeffler, Maftools: efficient and comprehensive analysis of somatic variants in cancer[J], Genome Res. 28 (11) (2018) 1747–1756.
[36] P. Geeleher, N. Cox, R.S. Huang, pRRophetic: an R package for prediction of clinical chemotherapeutic response from tumor gene expression levels[J], PLoS One 9 (9) (2014), e107468.
[37] G. Yang, W. Guan, Z. Cao, W. Guo, G. Xiong, F. Zhao, et al., Integrative genomic analysis of gemcitabine resistance in pancreatic cancer by patient-derived xenograft models[J], Clin. Cancer Res. 27 (12) (2021) 3383–3396.
[38] Q. Zhang, M.D. Green, X. Lang, J. Lazarus, J.D. Parsels, S. Wei, et al., Inhibition of ATM increases interferon signaling and sensitizes pancreatic cancer to immune checkpoint blockade therapy[J], Cancer Res. 79 (15) (2019) 3940–3951.
[39] F. Shi, B. Wei, T. Lan, Y. Xiao, X. Quan, J. Chen, et al., Low NLRP3 expression predicts a better prognosis of colorectal cancer[J], Biosci. Rep. 41 (4) (2021).
[40] M. Hergueta-Redondo, D. Sarrio, A. Molina-Crespo, D. Megias, A. Mota, A. Rojo-Sebastian, et al., Gasdermin-B promotes invasion and metastasis in breast cancer cells[J], PLoS One 9 (3) (2014), e90099.
[41] B.E. Bolivar, A.N. Brown-Suedel, B.A. Rohrman, C.I. Charendoff, V. Yazdani, J.D. Belcher, et al., Noncanonical roles of caspase-4 and caspase-5 in heme-driven IL-1beta release and cell death[J], J. Immunol. 206 (8) (2021) 1878–1889.
[42] G. Papoff, D. Presutti, C. Lalli, G. Bolasco, S. Santini, C. Manelfi, et al., CASP4 gene silencing in epithelial cancer cells leads to impairment of cell migration, cell-matrix adhesion and tissue invasion[J], Sci. Rep. 8 (1) (2018), 17705.
[43] S. Ruhl, K. Shkarina, B. Demarco, R. Heilig, J.C. Santos, P. Broz, ESCRT-dependent membrane repair negatively regulates pyroptosis downstream of GSDMD activation[J], Science 362 (6417) (2018) 956–960.
[44] J. Liu, R. Kang, D. Tang, ESCRT-III-mediated membrane repair in cell death and tumor resistance[J], Cancer Gene Ther. 28 (1–2) (2021) 1–4.
[45] A.K. Pfitzner, V. Mercier, X. Jiang, J. Moser von Filseck, B. Baum, A. Saric, et al., An ESCRT-III polymerization sequence drives membrane deformation and fission[J], Cell 182 (5) (2020) 1140–1155 e18.
[46] Y. Chen, Y. Liu, M. Wang, Identification of a pyroptosis-related gene signature and effect of silencing the CHMP4C and CASP4 in pancreatic adenocarcinoma[J], Int. J. Gen. Med. 15 (2022) 3199–3213.
[47] N. De Franceschi, M. Alqabandi, N. Miguet, C. Caillat, S. Mangenot, W. Weissenhorn, et al., The ESCRT protein CHMP2B acts as a diffusion barrier on reconstituted membrane necks[J], J. Cell Sci. 132 (4) (2018).
[48] J.Y. Zhang, B. Zhou, R.Y. Sun, Y.L. Ai, K. Cheng, F.N. Li, et al., The metabolite alpha-KG induces GSDMC-dependent pyroptosis through death receptor 6-activated caspase-8[J], Cell Res. 31 (9) (2021) 980–997.
[49] Y.Q. Cui, F. Meng, W.L. Zhan, Z.T. Dai, X. Liao, High expression of GSDMC is associated with poor survival in kidney clear cell cancer[J], BioMed Res. Int. 2021 (2021), 5282894.
[50] J. Wei, Z. Xu, X. Chen, X. Wang, S. Zeng, L. Qian, et al., Overexpression of GSDMC is a prognostic factor for predicting a poor outcome in lung adenocarcinoma [J], Mol. Med. Rep. 21 (1) (2020) 360–370.
[51] J. Ruan, Structural insight of gasdermin family driving pyroptotic cell death[J], Adv. Exp. Med. Biol. 1172 (2019) 189–205.
[52] Q. Sun, G. Fan, Q. Zhuo, W. Dai, Z. Ye, S. Ji, et al., Pin1 promotes pancreatic cancer progression and metastasis by activation of NF-kappaB-IL-18 feedback loop [J], Cell Prolif. 53 (5) (2020), e12816.
[53] M.N. Rossi, A. Pascarella, V. Licursi, I. Caiello, A. Taranta, L.R. Rega, et al., NLRP2 regulates proinflammatory and antiapoptotic responses in proximal tubular epithelial cells[J], Front. Cell Dev. Biol. 7 (2019) 252.
[54] J. Zhu, B. Tang, X. Lv, M. Meng, Q. Weng, N. Zhang, et al., Identifying apoptosis-related transcriptomic aberrations and revealing clinical relevance as diagnostic and prognostic biomarker in hepatocellular carcinoma[J], Front. Oncol. 10 (2020), 519180.
[55] K. Tsuchiya, Switching from apoptosis to pyroptosis: gasdermin-elicited inflammation and antitumor immunity[J], Int. J. Mol. Sci. 22 (1) (2021).
[56] H. Zhao, R. Wei, L. Wang, Q. Tian, M. Tao, J. Ke, et al., Activation of glucagon-like peptide-1 receptor inhibits growth and promotes apoptosis of human pancreatic cancer cells in a cAMP-dependent manner[J], Am. J. Physiol. Endocrinol. Metab. 306 (12) (2014) E1431–E1441.
[57] P. Gurung, P.K. Anand, R.K. Malireddi, L. Vande Walle, N. Van Opdenbosch, C.P. Dillon, et al., FADD and caspase-8 mediate priming and activation of the canonical and noncanonical Nlrp3 inflammasomes[J], J. Immunol. 192 (4) (2014) 1835–1846.

[58] R.E. Gutteridge, M.A. Ndiaye, X. Liu, N. Ahmad, Plk1 inhibitors in cancer therapy: from laboratory to clinics[J], Mol. Cancer Therapeut. 15 (7) (2016) 1427–1435.
[59] M. Chiappa, S. Petrella, G. Damia, M. Broggini, F. Guffanti, F. Ricci, Present and future perspective on PLK1 inhibition in cancer treatment[J], Front. Oncol. 12 (2022), 903016.
[60] S.E. Niklander, Inflammatory mediators in oral cancer: pathogenic mechanisms and diagnostic potential[J], Front Oral Health 2 (2021), 642238.
[61] Z. Gong, J. Ma, H. Su, T. Guo, H. Cai, Q. Chen, et al., Interleukin-1 receptor antagonist inhibits angiogenesis in gastric cancer[J], Int. J. Clin. Oncol. 23 (4) (2018) 659–670.
[62] H. Locy, S. de Mey, W. de Mey, M. De Ridder, K. Thielemans, S.K. Maenhout, Immunomodulation of the tumor microenvironment: turn foe into friend[J], Front. Immunol. 9 (2018) 2909.
[63] R.J. Torphy, R.D. Schulick, Y. Zhu, Understanding the immune landscape and tumor microenvironment of pancreatic cancer to improve immunotherapy[J], Mol. Carcinog. 59 (7) (2020) 775–782.
[64] Y.C. Hou, Y.J. Chao, M.H. Hsieh, H.L. Tung, H.C. Wang, Y.S. Shan, Low CD8(+) T cell infiltration and high PD-L1 expression are associated with level of CD44(+)/CD133(+) cancer stem cells and predict an unfavorable prognosis in pancreatic cancer[J], Cancers 11 (4) (2019).
[65] J.L. Carstens, P. Correa de Sampaio, D. Yang, S. Barua, H. Wang, A. Rao, et al., Spatial computation of intratumoral T cells correlates with survival of patients with pancreatic cancer[J], Nat. Commun. 8 (2017), 15095.
[66] L. Lu, H. Huang, J. Zhou, W. Ma, S. Mackay, Z. Wang, BRCA1 mRNA expression modifies the effect of T cell activation score on patient survival in breast cancer [J], BMC Cancer 19 (1) (2019) 387.
[67] L. Lu, Y. Bai, Z. Wang, Elevated T cell activation score is associated with improved survival of breast cancer[J], Breast Cancer Res. Treat. 164 (3) (2017) 689–696.
[68] I. Tirosh, B. Izar, S.M. Prakadan, M.H. Wadsworth 2nd, D. Treacy, J.J. Trombetta, et al., Dissecting the multicellular ecosystem of metastatic melanoma by single-cell RNA-seq[J], Science 352 (6282) (2016) 189–196.
[69] C. Fu, A. Jiang, Dendritic cells and CD8 T cell immunity in tumor microenvironment[J], Front. Immunol. 9 (2018) 3059.
[70] C.M. Rueda, M.E. Moreno-Fernandez, C.M. Jackson, S.G. Kallapur, A.H. Jobe, C.A. Chougnet, Neonatal regulatory T cells have reduced capacity to suppress dendritic cell function[J], Eur. J. Immunol. 45 (9) (2015) 2582–2592.
[71] V.P. Balachandran, M. Luksza, J.N. Zhao, V. Makarov, J.A. Moral, R. Remark, et al., Identification of unique neoantigen qualities in long-term survivors of pancreatic cancer[J], Nature 551 (7681) (2017) 512–516.
[72] L. Lu, W. Ma, C.H. Johnson, S.A. Khan, M.L. Irwin, L. Pusztai, In silico designed mRNA vaccines targeting CA-125 neoantigen in breast and ovarian cancer[J], Vaccine 41 (12) (2023) 2073–2083.
[73] H.B. Li, Z.H. Yang, Q.Q. Guo, Immune checkpoint inhibition for pancreatic ductal adenocarcinoma: limitations and prospects: a systematic review[J], Cell Commun. Signal. 19 (1) (2021) 117.
[74] L. Lu, E. Risch, R. Halaban, P. Zhen, A. Bacchiocchi, H.A. Risch, Dynamic changes of circulating soluble PD-1/PD-L1 and its association with patient survival in immune checkpoint blockade-treated melanoma[J], Int. Immunopharm. 118 (2023), 110092.
[75] M. Loos, N.A. Giese, J. Kleeff, T. Giese, M.M. Gaida, F. Bergmann, et al., Clinical significance and regulation of the costimulatory molecule B7-H1 in pancreatic cancer[J], Cancer Lett. 268 (1) (2008) 98–109.
[76] D.J. Birnbaum, P. Finetti, A. Lopresti, M. Gilabert, F. Poizat, O. Turrini, et al., Prognostic value of PDL1 expression in pancreatic cancer[J], Oncotarget 7 (44) (2016) 71198–71210.
[77] T. Daunke, S. Beckinger, S. Rahn, S. Kruger, S. Heckl, H. Schafer, et al., Expression and role of the immune checkpoint regulator PD-L1 in the tumor-stroma interplay of pancreatic ductal adenocarcinoma[J], Front. Immunol. 14 (2023), 1157397.
[78] X. Yang, C. Li, X. Liao, S. Liu, X. Li, X. Hou, et al., Paclitaxel induces pyroptosis by inhibiting the volume-sensitive chloride channel leucine-rich repeat-containing 8a in ovarian cancer cells[J], Oncol. Rep. 49 (6) (2023).
[79] C.C. Zhang, C.G. Li, Y.F. Wang, L.H. Xu, X.H. He, Q.Z. Zeng, et al., Chemotherapeutic paclitaxel and cisplatin differentially induce pyroptosis in A549 lung cancer cells via caspase-3/GSDME activation[J], Apoptosis 24 (3–4) (2019) 312–325.
[80] P. Wan, X. He, Y. Han, L. Wang, Z. Yuan, Stat5 inhibits NLRP3-mediated pyroptosis to enhance chemoresistance of breast cancer cells via promoting miR-182 transcription[J], Chem. Biol. Drug Des. 102 (1) (2023) 14–25.
[81] E. Petsalaki, M. Dandoulaki, G. Zachos, The ESCRT protein Chmp4c regulates mitotic spindle checkpoint signaling[J], J. Cell Biol. 217 (3) (2018) 861–876.
[82] J. Hou, R. Zhao, W. Xia, C.W. Chang, Y. You, J.M. Hsu, et al., PD-L1-mediated gasdermin C expression switches apoptosis to pyroptosis in cancer cells and facilitates tumour necrosis[J], Nat. Cell Biol. 22 (10) (2020) 1264–1275.
[83] J. Huo, Y. Shen, Y. Zhang, L. Shen, BI 2536 induces gasdermin E-dependent pyroptosis in ovarian cancer[J], Front. Oncol. 12 (2022), 963928.